Article:
Lou, Z., Min, X., Li, G. et al. (2 more authors) (2024) Advancing Sensing Resolution of Impedance Hand Gesture Recognition Devices. IEEE Journal of Biomedical and Health Informatics, 28 (10). 5855 -5864. ISSN 2168-2194

https://doi.org/10.1109/jbhi.2024.3417616

Advancing Sensing Resolution of Impedance Hand Gesture Recognition Devices

Zhiyuan Lou, *Student Member, IEEE*, Xue Min, Guanhan Li, James Avery, *Member, IEEE*, and Rebecca Stewart, *Member, IEEE*

***Abstract*— — Gestures are composed of motion information (e.g. movements of fingers) and force information (e.g. the force exerted on fingers when interacting with other objects). Current hand gesture recognition solutions such as cameras and strain sensors primarily focus on correlating hand gestures with motion information and force information is seldom addressed. Here we propose a bio-impedance wearable that can recognize hand gestures utilizing both motion information and force information. Compared with previous impedance-based gesture recognition devices that can only recognize a few multi-degrees-of-freedom gestures, the proposed device can recognize 6 single-degree-of-freedom gestures and 20 multiple-degrees-of-freedom gestures, including 8 gestures in 2 force levels. The device uses textile electrodes, is benchmarked over a selected frequency spectrum, and uses a new drive pattern. Experimental results show that 179 kHz achieves the highest signal-to-noise ratio (SNR) and reveals the most distinct features. By analyzing the 49,920 samples from 6 participants, the device is demonstrated to have an average recognition accuracy of 98.96%. As a comparison, the medical electrodes achieved an accuracy of 98.05%.**

***Index Terms*— Electrical impedance tomography, gesture recognition, machine learning, wearable sensor, textile technology**

I. Introduction

HAND gestures contain rich information and have been widely adopted as an interface for human-computer interaction [1]. Hand Gesture Recognition (HGR) devices have been developed based on machine vision [2], strain gauges [3], surface electromyography (sEMG) [4], and multimodal fusion methods such as machine vision-strain sensor fusion [5]. However, popularization of these devices are limited by a number of issues such as complex system architecture [5], physically constraining user's finger movement [6], requirements for high-quality materials [7], [8], and sensitivity to user's environment [9]. For example, complicated backgrounds and dark/unbalanced lighting lead to a decay in recognition accuracy in machine vision HGR devices [9]. The sEMG signal has an inherently low signal-to-noise ratio (SNR) and so is sensitive to environmental noise [10]. Large-area, high-density wet electrode arrays mitigate the problem [4], [11], but are cumbersome and add extra system complexity.

In recent years, attempts have been made to use electrical impedance tomography (EIT) as an alternative solution to HGR [12]–[17]. In EIT measurements, boundary voltage measurements are used to infer the inner impedance distribution and the inner structure of the object [18]. In the case of HGR, EIT is used to detect the muscle and surrounding tissue shape changes in the forearm [13]. However, EIT gesture recognition is challenging as the EIT image reconstruction is a highly nonlinear, ill-conditioned, and uncertain problem [19]. Limited by the EIT resolution, recognizing small motion is difficult and the current EIT HGR approach can only recognize a small number of multiple-degree-of-freedom (DoF) hand gestures [12], [13], [15]–[17]. To recognize more hand gestures, the dataset needs to be split into sub-groups each with their own dedicated machine learning model, which adds complexity to the system [14].

In addition to the factors discussed above, most of the current HGR devices correlate gestures with movements of the fingers [2]–[8], [12]–[17], and the force applied by the fingers is seldom addressed. Some gestures involve the same finger motion but with different forces, such as pinching with a low force and high force, which are hard to differentiate with the current HGR solutions. However, the force information from the hand has great potential in multiple domains such as enhancing performance in human-robot collaboration, and providing new forms of interactions in virtual reality. For example, Zheng et al. demonstrated a human-robot sawing task using grasp force estimated from EIT [20]. With the per-finger force information from hand gestures, more dexterous human-robot collaborations can be achieved.

Here we report an electrical impedance HGR system. Compared with the high-density sEMG approach that uses 64 wet electrodes [4], the system has less complexity and is less cumbersome when worn, featuring only 8 dry textile electrodes. Whereas recognizing small motions (e.g., single degree

Zhiyuan Lou is with the Dyson School of Design Engineering, Imperial College London, London, SW7 2BX, UK (e-mail: z.lou22@imperial.ac.uk).

Xue Min is with the School of Design, Jiangnan University, Wuxi, 214122 China and also with the Dyson School of Design Engineering, Imperial College London, London, SW7 2BX, UK (email: x.min22@imperial.ac.uk).

Guanhan Li is with the Department of Aeronautics, Imperial College London, London, SW7 2BX, UK (e-mail: guanhan.li23@imperial.ac.uk).

James Avery is with the School of Electronic and Electrical Engineering, University of Leeds, Leeds, LS2 9JT, UK (e-mail: j.p.avery@leeds.ac.uk).

Rebecca Stewart is with the Dyson School of Design Engineering, Imperial College London, London, SW7 2BX, UK (e-mail: r.stewart@imperial.ac.uk). *(Zhiyuan Lou and Xue Min are co-first authors)(Corresponding author: Zhiyuan Lou)*

of freedom hand gestures) is challenging for conventional EIT HGR devices, the proposed system can recognize the position of each individual finger. Additionally, the system can recognize hand gestures based on differing forces exerted by each finger.

The aim of this study is to propose a hand-based impedance gesture recognition system and validate if it is capable of accurately recognizing both motion-related and force-related gestures. The first part of the study is parameter optimization, in which 3 subjects were recruited. To optimize the frequency of the electrical impedance device, we recorded the impedance signal at a frequency spectrum ranging from 1 kHz to 364 kHz and calculated the SNR and distinguishability of the signal. Then we proposed an opposite current injection-voltage measurement drive pattern and compared its performance with the classical adjacent drive pattern. The second part of the study implements gesture recognition and machine learning using these selected parameters (i.e. frequency and drive pattern), in which 6 subjects were recruited. We validated gesture recognition performance with a 1-Dimensional Convolutional Neural Network (1D-CNN) model on a 26-hand gesture dataset, using both the proposed system and medical electrodes.

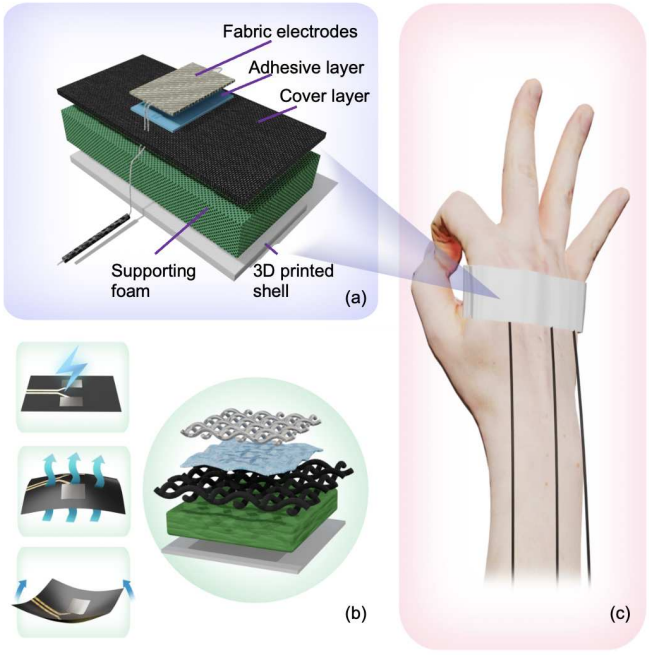

Fig. 1. System overview (a) One sensing unit of the device. (b) Structure of the electrodes. The fabric electrodes is highly conductive, breathable and soft. (c) Device on the hand

II. Gesture Recognition System

A. Device Overview

Figure 1(a) illustrates the basic sensing unit, which is composed of a textile electrode, adhesive layer, textile cover layer, foam support layer, and a 3D-printed hard shell. Fig. 1(b) visualizes the microstructure of the textiles. The electrodes are made of conductive fabric (ShieldEx Technik, tex-P180+B). Shieldex Technik-tex P180+B is a mirror-satin knitted fabric using 94% polyamide and 6% Dorlastan, with 99.9% pure silver plating. The structure of the fabric is suitable for applications that require homogeneous current distribution such as electrodes. The silver plating ensures an electrical surface resistivity smaller than 2Ω/sq. The fabric also demonstrates good bio-compatibility [21] and washability [22]. The soft textile layer, foam layer, and 3D-printed shell help to maintain constant contact with the skin. They also help to minimize the movement of the electrodes, and thus reduce the motion artifacts. Fig. 1(c) shows the device on the hand. Eight textile electrodes are used, with 4 electrodes evenly placed on the back of the hand and 4 electrodes evenly placed on the palm. An impedance spectrometer (Eliko Quadra Impedance Spectroscopy) is used to inject current and measure voltage [23]. The impedance data is calculated and processed in the spectrometer and then transmitted to a PC via the universal serial bus for machine learning and gesture recognition.

B. Hand Anatomy and Design Considerations

Muscles on the forearm and hand contribute to the actuation of fingers. In the forearm, finger flexor muscles are densely packed and adjacent to each other, as shown in Fig. 2(a). For example, the four tendons assisting the motion of digits 2-5 merge at the same muscle, the flexor digitorum superficialis. The low spatial resolution of EIT makes it hard to locate the exact muscle fascicles in the flexor digitorum superficialis that contribute to the motion of a specific digit. Thus, identifying the flexion of one single finger is challenging for conventional EIT setups [12], [13]. Meanwhile, the contraction of the muscles and movement of the tendons will change the forearm boundary shape [24]. Solving the imaging reconstruction problem in EIT assumes the boundary of the body is known a priori, and small errors in boundary shape can lead to large systematic artifacts [25]. Based on these two factors, HGR with small motion and/or large hand gesture datasets is intrinsically challenging for the EIT approach on the forearm.

Muscles on the hand are spatially set apart to actuate individual fingers, as shown in Fig. 2(b). For example, the second and the third dorsal interosseous muscle flexes the middle finger, while the first dorsal interosseous muscle and the first palmar interosseous flexes the index finger. These inner muscle contractions lead to inner impedance distribution changes. Moreover, the contraction of the muscle alters the hand boundary shape, which can be reflected as further changes in the impedance signals. We validated the change in the hand shape and its inner structure by reconstructing the cross-sectional view of the hand Magnetic Resonance Imaging (MRI) dataset [26], as demonstrated in Fig. 2(c). As the hand boundary shape differs, we use raw electrical impedance signals for gesture recognition, rather than trying to reconstruct tomography images. We recognize the measured impedance change as a complex combination of the noise from hardware, contact impedance change, and tissue impedance change caused by both inner tissue deformation and outer shape deformation.

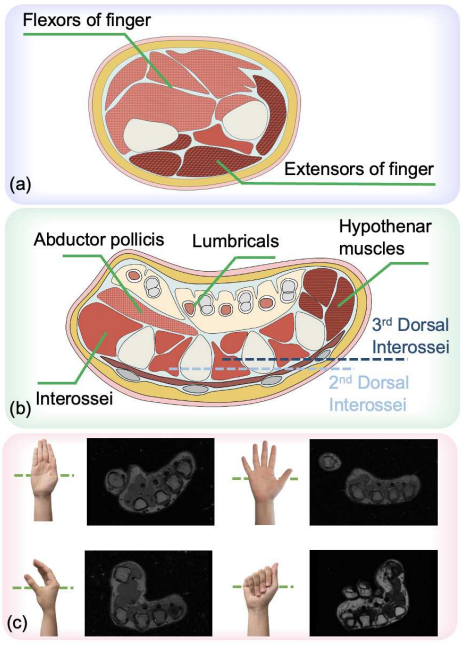

Fig. 2. (a) Arm anatomy (b) Hand anatomy (c) Reconstructed hand MRI image. The hand boundary shape and inner structure change across different hand gestures.

C. Gestures

We created a hand gesture dataset that contains both commonly used single-degree-of-freedom (single-DOF) gestures [4] and a subset from American Sign Language (ASL) [27]. In addition to the conventional thumb-to-finger pinch set [28], [29], we also added 4 hard pinches, which require participants to apply as much force as they can. As shown in Fig. 5, the final hand gesture dataset consists of 26 hand gestures, with 6 single-DOF hand gestures and 20 multi-DOF hand gestures. The 20 multi-DOF hand gestures contain 12 ASL gestures and 8 pinch gestures with two differing levels of force. The data collection methodology was approved by the Imperial College London Science, Engineering, and Technology Research Ethics Committee (Application 6704836).

III. Experimental Methods

A. Frequency Selection

Since the impedance response is strongly correlated with the frequency of injecting current [30], [31], it is important to first identify the optimal frequency for this application. Two factors are considered in the frequency selection phase: the SNR and the distinguishability of the EIT signal under different hand gestures. To evaluate these parameters, we built a simplified EIT model with two medical electrodes evenly placed on the back of the hand and two electrodes evenly placed on the palm in the opposite position, as shown in Fig. 3. This four-electrode setup constitutes a single sensing unit of the full eight-electrode EIT measurement scheme. Two electrodes on the back of the hand inject the current and two electrodes on the palm measure the voltage. Standard Ag/AgCl electrodes (TIANRUN SUNSHINE Medical Supplies Co. Ltd.) were used for this process. The impedance data is recorded with

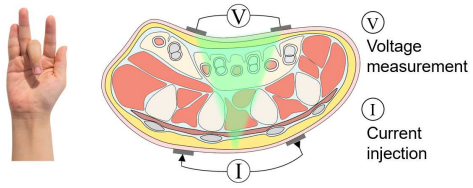

Fig. 3. Frequency selection setup. Two electrodes are evenly placed on the palm and back of hand respectively. A frequency sweep is performed while the participant performs single-DOF gestures.

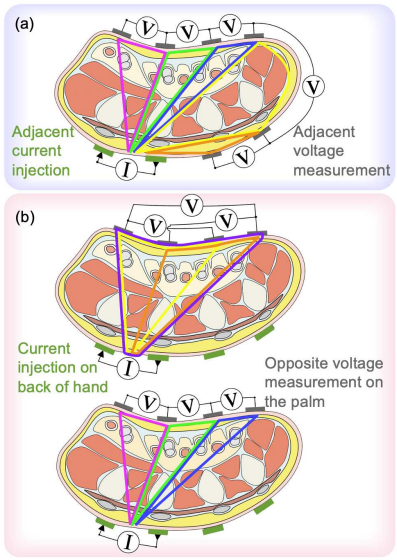

Fig. 4. (a) Conventional adjacent drive pattern. (b) Proposed opposite drive pattern.

a current injection frequency spectrum ranging from 1 kHz to 364 kHz generated by the Eliko impedance spectrometer.

The first factor, SNR, is calculated when the hand is in the neutral state. and is defined as the ratio of the mean value of the impedance signal to the standard deviation of the impedance signal. The second factor, the distinguishability of the signal, is quantified by the average impedance change observed when the middle finger bends, a basic hand gesture component. The process is repeated on the right hands of three subjects (hand width 7cm-10cm) with 200 measurements each.

B. Injection-Measurement Drive Pattern

The distinguishability of the EI signal is related to the SNR and the probability of detecting impedance changes, which is strongly related to the current injection-voltage measurement pattern [32]. Fig. 4 shows the adjacent injection-measure scheme, the most common drive pattern in four-electrode EIT measurements [33]. In this measurement scheme, two adjacent electrodes are used to inject current, and two other adjacent electrodes are used to measure the voltage. This process is repeated for all possible combinations. For 8 electrodes, the full loop contains 40 measurements.

The adjacent drive pattern utilizes neighboring electrode pairs in both current injection and voltage measurement, whose relative position changes are small across different hand

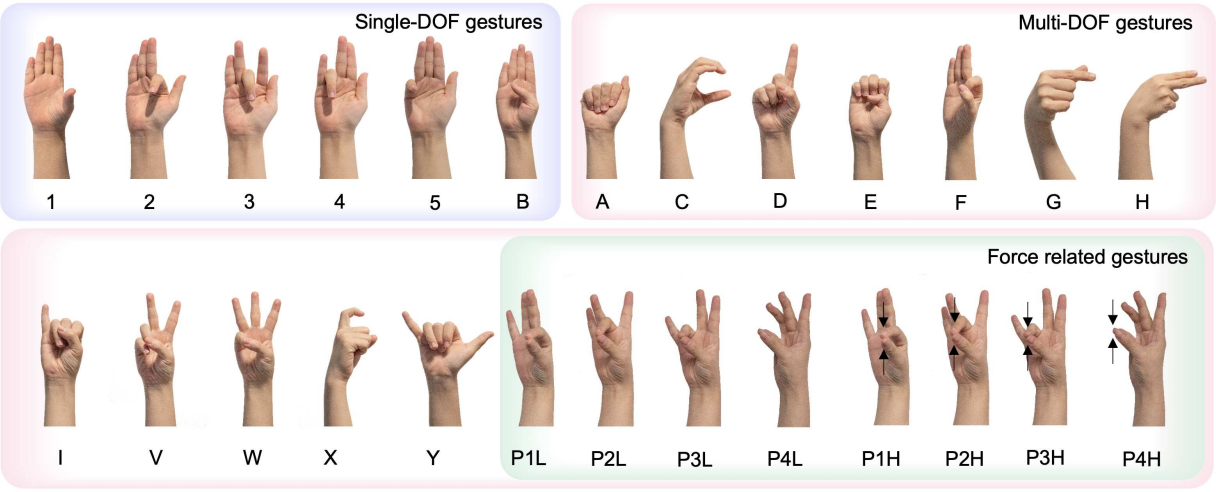

Fig. 5. Hand gesture dataset. The dataset contains 6 single-DoF gestures and 20 multi-DoF gestures, among which are 8 force-related gestures.

gestures. Also, simulation results show the distinguishability of impedance signals increases with interface pattern angle and low angle interface patterns such as adjacent patterns are a poor choice [32]. Thus, the adjacent injection-measurement pattern may be suboptimal in capturing the hand gesture features. To address this issue, we proposed an opposite drive pattern, as shown in Fig. 4. The proposed approach injects currents on the back of the hand, measures the voltage on the palm, and exhausts all possible electrode combinations. The proposed injection measurement pattern contains $C_4^2 \times C_4^2 = 36$ current injection - voltage measurements.

To validate, we collected a dataset of 31,200 samples, which constituted 26 gestures with 200 measurements on each gesture from three subjects (hand width 7cm-10cm). Using this dataset, we calculated the separability criterion J, a typical method to evaluate class separability [34]:

$$J = \frac{tr(S_B)}{tr(S_W)} \tag{1}$$

where S_W is the within-class scatter matrix and S_B is the between-class scatter matrix. These can be calculated by:

$$S_W = \sum_{i=1}^{c}[\sum_{j=1}^{n_i}(x_{i,j} - m_i)(x_{i,j} - m_i)^T] \tag{2}$$

$$S_B = \sum_{i=1}^{c} n_i(m_i - m)(m_i - m)^T \tag{3}$$

in which c is the number of classes, n_i is the number of samples in the i-th class, $x_{i,j}$ is the j-th sample in the i-th class, m is the mean vector of all the samples and m_i is the mean vector of the samples in the i-th class. If a dataset has a large between-class scatter and a small within-class scatter (i.e., higher J), the dataset has better separability. To further visualize the result, we also performed the t-Distributed Stochastic Neighbor Embedding (t-SNE) on the data from each subject.

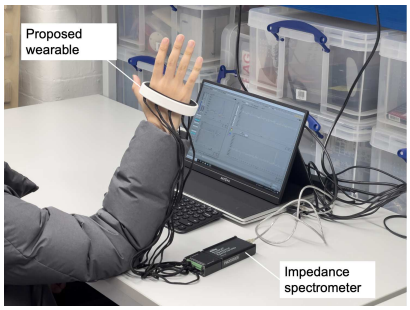

Fig. 6. Impedance data collection setup.

C. Gesture Dataset Collection and Machine Learning

Six participants were recruited in the data collection process (hand width 7cm-10cm). Due to the differences in hand size, electrode placements were adjusted so that the electrodes were evenly spaced across each participant's hand.

Our study had two data collection phases. In phase 1, data with conventional Ag/AgCl medical electrodes was collected as a "gold standard". Each participant was asked to hold each gesture for 6 seconds, during which time 40 samples were recorded. One round of data collection consisted of all 26 gestures. In total, we collected four rounds of data for each participant with medical electrodes. In phase 2, the data collection process was repeated using the proposed wearable and was scheduled on a different day to avoid fatigue. In summary, the phase 1 and phase 2 data collection yield 49,920 samples (6 participants × 40 samples × 26 gestures × 4 rounds × 2 materials).

Since the input data to the machine learning model is not a time series, we used a 1-dimensional convolutional neural network (1D-CNN) as the machine learning model, instead of models such as long short-term memory (LSTM). The 1D-CNN model was built in Python (Version 3.10.12), with the TensorFlow library (Version 2.15.0) [35]. Fig. 7 visualizes the model, which consists of 4 convolutional layers, 2 max-pooling layers, and 3 dense layers. We also performed data augmentation on the dataset. The proposed drive pattern con-

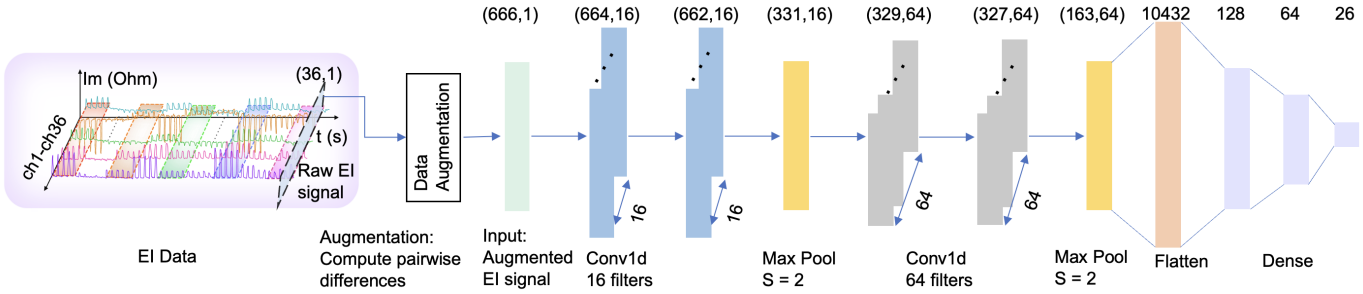

Fig. 7. Proposed 1-D CNN Structure. The original dataset contains 36 channels of data. Data augmentation is performed by computing the difference between these 36 channels, which are then combined with the original data and fed to the 1D CNN model.

tains 36 injection-measurement pairs. Then we computed the difference of these measurement pairs, which yield $C_{36}^2 = 630$ additional features. In total, there are 666 features.

The 666 electrical impedance signal are fed into two consecutive 1D convolutional layers (filters = 16, kernel size = 3), followed by a max pooling layer (pool size = 2). The convolutional layers detect and extract higher-level features from the input and generate a feature map. The following max pooling layer reduces the spatial dimensions of the feature map and creates a down-sampled version by taking the maximum value in each pooling region. The weights of these layers are initialized with Glorot uniform initializer, which provides faster convergence than random initializer in deep neural networks [36]. A further block of 2 convolutional layers (filters = 64, kernel size = 3) was then used, followed by the max pooling layer (pool size = 2).

The model is trained using 70% of the data (i.e. training dataset). Another 15% of the data (i.e. validation dataset) is utilized for hyperparameter tuning during the training phase. The remaining 15% of the data (i.e. test dataset) is held out from the model throughout training for unbiased evaluation of the model's performance. To account for individual variations in hand anatomy, the model was trained, validated and tested on each participant's data separately.

IV. Experimental Results

A. Frequency Selection

Fig. 8(a) shows the SNR over the frequency spectrum. The SNR increases with frequency and starts to converge after 127 kHz. Fig. 8(b) shows the mean impedance change generally stabilizes after 179 kHz. Considering both factors, 179 kHz is selected as the excitation frequency.

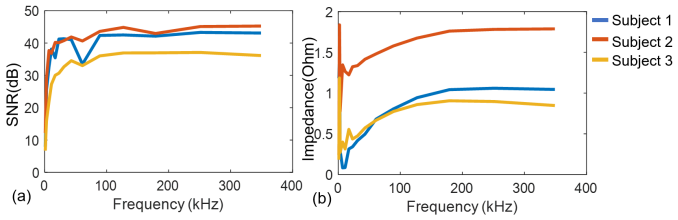

Fig. 8. (a)SNR and (b)Distinguishability (i.e. characterized by mean impedance change) of the hand gesture impedance signal.

B. Influence of the Injection-Measurement Drive Pattern

Fig. 9 shows the separability J calculated from three subjects. The opposite drive pattern has a 56.3% higher mean separability criterion compared to that of the adjacent drive pattern. This demonstrates the opposite drive pattern increases the ratio of between class distance and within class distance. Thus, the opposite drive pattern is more feasible for hand gesture recognition.

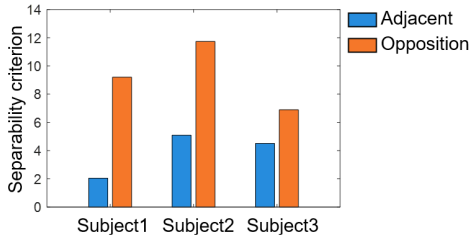

Fig. 9. Separability criterion across different subjects

t-SNE is used to visualize the high dimensional input impedance data. As shown in Fig. 10, the proposed drive pattern shows better clustering results than the adjacent drive pattern. However, there are still several hand gesture groups that cannot be distinguished by the t-SNE method such as gesture "P4L" and gesture "W". These two groups have a large number of samples that overlap with each other. Thus, we used a 1D-CNN model for further gesture classification.

Fig. 11 shows the time series hand gesture data with the proposed drive pattern. Each gesture is repeated 5 times. The time series signal suggests good repeatability and low drift over time with the proposed drive pattern.

C. Gesture Classification

We compared the 1D-CNN gesture recognition results with other machine learning algorithms, such as support vector machines (SVMs), bagged trees, random under sampling (RUS) trees, and random forests. To control variables, we used the same input data (i.e. impedance signal) and followed the same data processing procedure. The output for these models is predicted hand gestures. Table I shows the average model performance across six participants. The machine learning models generally demonstrated high accuracy, precision, recall, and f-score values. Among them, the proposed wearable with 1D CNN achieved the highest recognition accuracy of 98.96%.

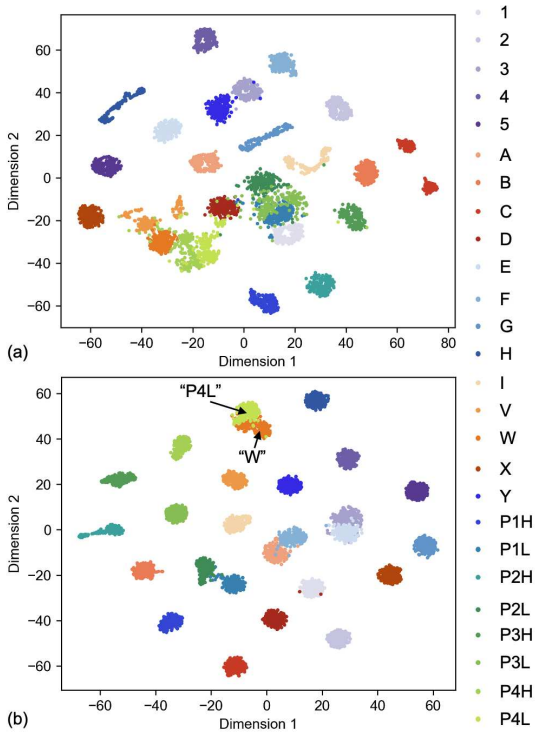

Fig. 10. t-SNE results for (a) adjacent and (b) opposite drive pattern

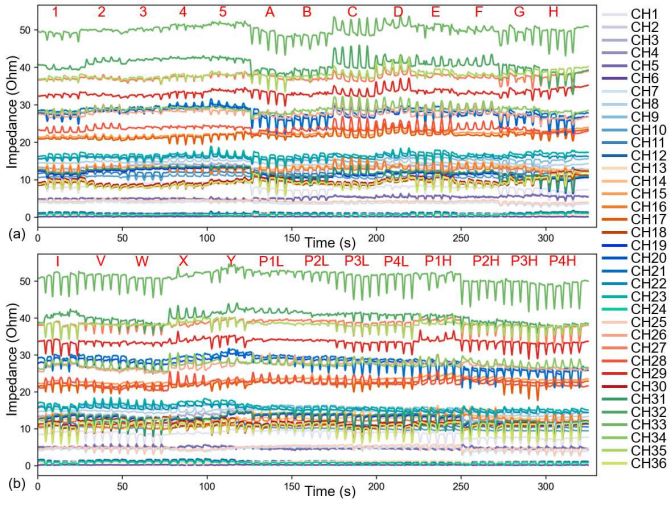

Fig. 11. Time series hand gesture data. (a) Gesture 1-H. (b) Gesture I-P4H.

To validate if the model overfits the dataset, we plotted the training and validation loss curve for each participant's data. Both curves show a downward trend that stabilizes, suggesting a good fit. The closeness of the two curves at the end of training suggests the model generalizes well on unseen data. Wilcoxon signed rank test was conducted to test if there is a statistical difference between medical and textile electrodes. All the machine learning algorithms yielded a p-value greater than 0.05. Thus, despite the textile electrodes having a higher average recognition accuracy, the difference is not statistically significant.

TABLE I
MODEL PERFORMANCE OF 5 ALGORITHMS

	Accuracy	*Precision*	*Recall*	*f-Score*	*p value*
SVM (Medical)	97.81%	97.94%	97.81%	0.9777	
SVM (Textile)	98.16%	98.37%	98.16%	0.9814	0.753
Bagged Trees (Medical)	97.33%	97.46%	97.33%	0.9733	
Bagged Trees (Textile)	97.57%	97.89%	97.57%	0.9750	0.753
RUS Boosted Trees (Medical)	96.87%	97.22%	96.88%	0.9692	
RUS Boosted Trees (Textile)	98.61%	98.76%	98.61%	0.9864	0.686
Random Forest (Medical)	97.70%	97.91%	97.70%	0.9771	
Random Forest (Textile)	98.16%	98.33%	98.16%	0.9813	0.833
1D CNN (Medical)	**98.05%**	**98.23%**	**98.05%**	**0.9804**	
1D CNN (Textile)	**98.96%**	**99.10%**	**98.96%**	**0.9897**	**0.248**

V. DISCUSSION

A. Location Considerations

We extracted the common light pinch gestures from the dataset collected on the hand and compared it with datasets collected on arm, wrist, and wrist-back of hand locations [12], [37]. As shown in Fig.12, the accuracy on the hand is 22.68% higher than the arm, 14.88% higher than the wrist, and 2.51% higher than wrist-back of hand. We infer the hand provides richer hand gesture impedance information than the arm/wrist due to its anatomical structure. All prime movers are located in the hand for some gestures such as the little finger pinch. For this gesture, the thumb is primarily actuated by the opponens pollicis, flexor pollicis brevis and abductor pollicis brevis, while the little finger is primarily actuated by the opponens digiti minimi and flexor digiti minimi brevis [38]. Muscles on the arm do not extensively participate in this gesture, which may be a reason that arm/wrist based solution has lower recognition accuracy.

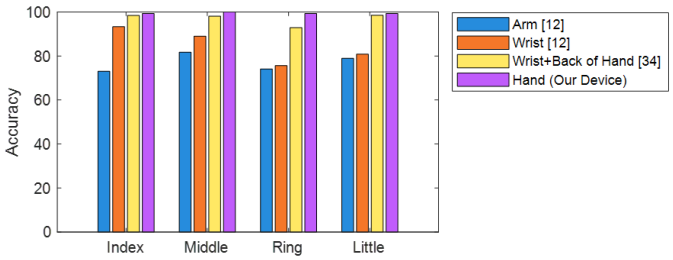

Fig. 12. Pinch gesture (i.e., P1L-P4L) recognition accuracy in arm [12], wrist [12], wrist-back of hand [37] and hand (our device).

B. Impedance Measurement Parameters

We investigated frequency and drive pattern, two of the most important parameters for impedance based gesture recognition. For frequency, previous works often adopt lower frequencies such as 20kHz [17], 40kHz [12], and 50kHz [13] as the impedance measurement hardware was designed around AD5933 impedance analyzer [39], which limits the excitation frequency below 100kHz. However, in traditional impedance

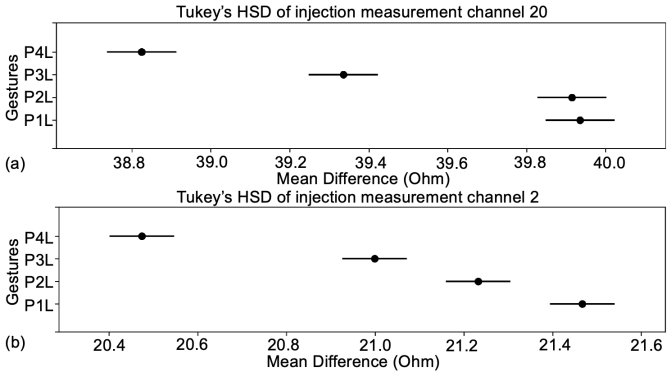

Fig. 13. Tukey's HSD for data collected on subject 1 with the proposed wearable with (a) Injection-measurement channel 20 and (b) Injection-measurement channel 2.

tomography applications, larger EIT bandwidth appears to be important [40]. For example, Kerner reported the optimal breast EIT images at 950kHz [41]. Thus, we measured the SNR and mean impedance difference change at frequencies ranging from 1kHz to 349kHz, the largest bandwidth supported by the Eliko impedance spectrometer. Experimental results show the SNR stabilized after 127kHz and the mean impedance difference stabilized after 179kHz. Since higher frequencies are potentially more sensitive to parasitic capacitances in the wiring, we chose 179kHz as the carrier frequency in subsequent gesture recognition applications.

Alongside frequency, drive pattern is another important factor that influences the both the data and reconstructed image quality in conventional EIT. Previous studies show the adjacent drive pattern results in high image resolution [42] but its distinguishability is sub-optimal [43]. The proposed cross drive pattern outperforms the adjacent pattern in distinguishability, a more important indicator in gesture recognition applications.

C. Gesture Dataset Analysis

The data analysis was conducted from two viewpoints: (1) from within users using Analysis of Variance (ANOVA) test and Tukey's Honest Significance Difference (HSD) test to understand if there are any statistically significant differences between the impedance changes of different gestures; (2) considering across users, feature importance (FI) analysis is performed to understand if there are large individual differences in the electrical impedance signals.

For the ANOVA test, the resulting p-value is smaller than 0.05 (6.86e-27), indicating a high statistically significant difference between different hand gestures. Tukey's HSD test was performed to check the pairwise statistical gesture impedance differences. Results show the pairwise statistical difference depends on drive pattern and different injection measurement channels reveal different aspects of the hand gesture features. To illustrate an example, Tukey's HSD results on light pinch gestures from channel 20 and channel 2 are plotted in Fig. 13. In this type of Tukey's HSD plot, if confidence intervals of two group means do not overlap, there is a statistically significant difference between them [44]. It can be seen that gesture P1L and P2L are very similar when measured at injection-measurement channel 20 (large overlap) but very different to channel 2 (no overlap). Thus, channel 2 might contribute more to classify P1L and P2L in subject 1's dataset. The result indicates when classifying specific gestures (e.g., P1L and P2L), further optimizations can be done by reducing certain injection measurement channels (e.g. channels similar to channel 20) while increasing others (e.g. channels similar to channel 2).

Feature importance (FI) is calculated using each participant's original 36-channel data using a random forest model [45]. FI provides indications of features that have the most influence on the model's predictions. As shown in Fig. 14, FI differs across the 6 subjects. For example, among the top 10 most important features, there are no common injection-measurement pairs between subjects 1 and 2, and only 4 common pairs (i.e., channel 31, 32, 35, and 36) between subjects 2 and 3. The results indicate there may exist large individual differences in the hand electrical impedance signal.

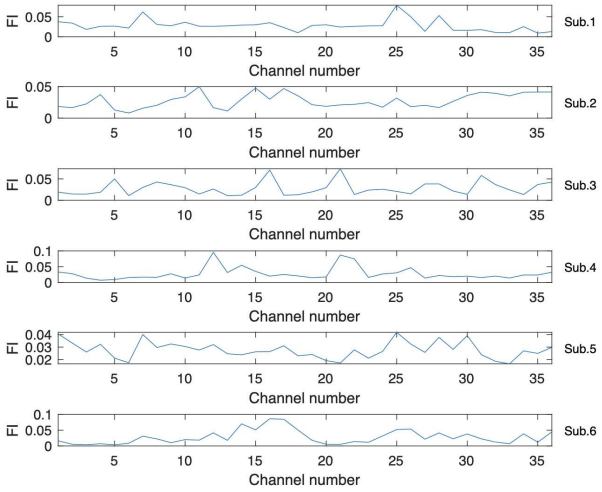

Fig. 14. Feature importance calculated from 6 subjects data.

D. Gesture Recognition

Fig. 15 shows the confusion matrix of the gesture classification with medical electrodes and our wearable device respectively. We randomly selected 15% of the data to comprise the independent test dataset. The number of samples in each class is balanced. Thus, for 6 participants, the total number of samples in each class is 144 (i.e. 40 samples × 4 rounds × 6 participants × 15%). The gesture recognition accuracy of the medical electrodes dataset is 98.05±2.39% and 98.96±1.37% for the textile electrodes dataset. Misclassifications occur in very similar hand gestures. For medical electrodes, gesture groups with the highest recognition error rates are ASL gesture "F" and light pinch gesture 1 (i.e. pinch with thumb and index finger with low force). These two gesture groups are very similar except that the pinch gesture tends to bend the index finger, middle finger and ring finger in a more natural state. For the textile wearable, gesture groups with the highest recognition error rates are ASL gestures "W" and "V". They are also similar with the only difference being the ring finger bends down for "V" while straightens up for "W".

This article has been accepted for publication in IEEE Journal of Biomedical and Health Informatics. This is the author's version which has not been fully edited and content may change prior to final publication. Citation information: DOI 10.1109/JBHI.2024.3417616

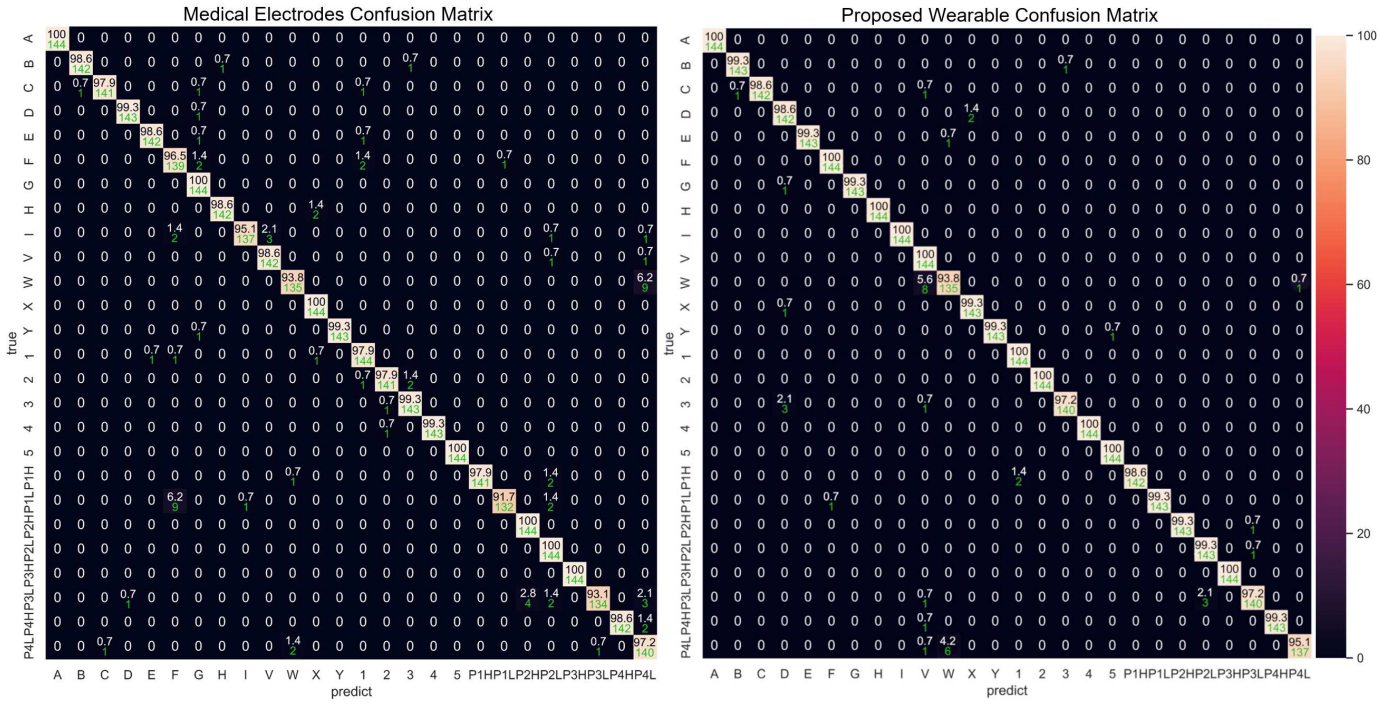

Fig. 15. Confusion matrix for medical electrodes and proposed wearable on test dataset. Number of samples is balanced on each class (i.e. 144) in the test dataset. The average gesture recognition accuracy across 6 participants is 98.05% and 98.96% respectively.

On the material side, the proposed device has a higher accuracy than "gold standard" medical electrodes on average, but it is not statistically significant. This means that the proposed device was able to match the classification accuracy of the gold standard medical electrodes, with the benefits of greater convenience to the user. This result aligns with previous studies showing textile electrodes have higher contact impedance, which contribute to larger impedance changes when the user performs different hand gestures [15]. However, a larger study with more users will be needed to confirm this is the case for our device.

E. Model Generalization

The performance of the machine learning models on unseen data is considered both in terms of within-user and cross-user generalization. In the within-user case, we used 15% of data that is not involved in the 1D-CNN model training process to evaluate model fit. The recognition accuracy is high (i.e. 98.96%).

In the cross-user case, the leave-one-participant-out validation scheme was used. We trained the 1D-CNN model using five participants' data and used data from the sixth participant to evaluate model fit. We extracted the pinch gesture dataset and compared the cross-user gesture recognition accuracy with previous work [12]. Five participants' data was used to train the 1D-CNN model and the sixth participant's data was used to test the model. On average, the cross-user accuracy is 30.58±6.98%. In contrast, Zhang et al reported 48.8% cross-user accuracy on the arm and 40.2% on the wrist [12]. The reason for this low cross-user accuracy may be the large individual differences as indicated by feature importance distribution. Specific reasons may include: (1) participants have different hand sizes and a wearable was customized for each subject; (2) some participants may perform the gestures in a non-standard way; (3) the dataset only contains 6 subjects, whereas Zhang et al used a dataset containing 10 subjects. In summary, the results indicate that the 1-CNN model is not universal at the scale of the dataset we collected. Thus expanding the dataset is one possible solution to improve the model generalization.

F. Comparison with Other Works

A comparison with other works has been listed in Table II. Whereas most current gesture recognition solutions recognize hand gestures based on position information, our device is able to recognize gestures with same shape but different force. This provides an alternative to the recently proposed photoplethysmography (PPG) and sEMG-based simultaneous hand gesture and force classification [46], [47].

In addition, the proposed device also has a smaller form factor than HGR gloves and allows users to freely move their fingers [27]. The design allows the user to put on and take off the device easily. In contrast, many HGR devices that utilize wet electrodes or strain sensor tattoos [7] require cumbersome preparation steps and can only be used once.

Compared with the previous EI/EIT based HGR device that can recognize limited hand gestures (< 10 with one machine learning model) [12]–[17], our EI HGR device has extended gesture recognition capability and can recognize 26 gestures with one machine learning model. Also, this device is able to recognize small motions and 6 single degree of freedom hand gestures.

TABLE II
COMPARISON WITH OTHER WORKS

Mechanism	Device	Location	Classification Method	Sensor Num	Gestures	Force Related	1Dof Gestures	Accuracy	Ref
Piezo-resistive	Glove	Hand	Amplitude	9	26	No	Yes	NA	[27]
PPG	Wrist band	Wrist	SVM	1	12	Yes	No	77.5%	[46]
sEMG	Patch	Arm	Hyperdimensional Computing	64	13 or or 21	No	Yes	97.12% or 92.87%	[4]
EIT	Armband	Arm	DNN	8	5+5+5+5	No	No	Train together:<60% Subgrouping:98%	[14]
EIT	Armband	Arm	SVM	8	3	No	No	95%	[15]
EIT	NA	Arm	CNN	8	10	No	No	95.94%	[16]
EI	NA	Wrist + Hand	SVM	5	6 or 6	No	No	98.7% or 97.8%	[37]
EI	Hand band	Hand	CNN	8	26	Yes	Yes	Train together: 98.96%	This work

G. Limitations and Future Work

In the future, we see several potential applications for this device, such as grasp force assessment and human-robot collaboration enhancement, both of which would benefit from a wider gesture classification and additional force estimation. However, some limitations need to be addressed before taking the device to real-world applications. First, current cross-user accuracy is quite low. One potential solution may be few-shot transfer learning. By tuning the learning rate of each layer of the current CNN model [48] and using a few samples from a new user, the model may be able to adapt quickly and achieve relatively high accuracy in the new user. Second, the current model has 1,360,276 parameters and runs on a PC (CPU i5 12400, GPU RTX 3060). To minimize the system, it is possible to transfer the model to embedded platforms by reducing the number of layers and performing model compression with methods like model quantization [49]. Third, we currently only classify two force levels. It might be interesting to test with more force levels and more precise force level evaluated with maximal voluntary contraction [46]. Fourth, a deeper investigation into the relationship between the drive pattern and pairwise statistically significant differences in the gesture dataset may further help to optimize the drive pattern. As indicated by Tukey's HSD results, the injection-measurement pairs contribute unevenly to the hand gesture classification. Based on target gestures to be recognized, specific optimizations on the drive pattern can be made.

In addition, we selected textiles to fabricate the system since it is a material for everyday use and is observed to be more comfortable to wear than wet medical electrodes. However, no formal assessments have been performed regarding the wearability and comfort of the device. In the future, usability surveys such as System Usability Scale (SUS) can be conducted as to better characterise the current device and guide further iterations [50].

VI. CONCLUSION

We developed a textile impedance-based hand gesture recognition device by optimizing the frequency and drive pattern. The hand band design allows the user to freely move the fingers and interact with other objects. We evaluated the SNR and distinguishability of the EI signal across a wide frequency spectrum and selected 179 kHz as the preferred frequency for hand-based EI HGR applications. In addition, we proposed a new drive pattern (opposite drive pattern) that outperformed the conventional adjacent drive pattern used in hand-based EI HGR applications.

Our device was able to recognize hand gestures with small motion and hand gestures with different forces. With the proposed new drive pattern, the wearable device can achieve an accuracy of 98.96% in 26 hand gestures, whereas the medical electrodes achieved an accuracy of 98.05%.

VII. REFERENCES

[1] R. Yin, D. Wang, S. Zhao, Z. Lou, and G. Shen, "Wearable sensors-enabled human–machine interaction systems: from design to application," *Advanced Functional Materials*, vol. 31, no. 11, p. 2008936, 2021.

[2] T. Starner, J. Weaver, and A. Pentland, "Real-time american sign language recognition using desk and wearable computer based video," *IEEE Transactions on pattern analysis and machine intelligence*, vol. 20, no. 12, pp. 1371–1375, 1998.

[3] O. A. Araromi, M. A. Graule, K. L. Dorsey, S. Castellanos, J. R. Foster, W.-H. Hsu, A. E. Passy, J. J. Vlassak, J. C. Weaver, C. J. Walsh *et al.*, "Ultra-sensitive and resilient compliant strain gauges for soft machines," *Nature*, vol. 587, no. 7833, pp. 219–224, 2020.

[4] A. Moin, A. Zhou, A. Rahimi, A. Menon, S. Benatti, G. Alexandrov, S. Tamakloe, J. Ting, N. Yamamoto, Y. Khan *et al.*, "A wearable biosensing system with in-sensor adaptive machine learning for hand gesture recognition," *Nature Electronics*, vol. 4, no. 1, pp. 54–63, 2021.

[5] M. Wang, Z. Yan, T. Wang, P. Cai, S. Gao, Y. Zeng, C. Wan, H. Wang, L. Pan, J. Yu *et al.*, "Gesture recognition using a bioinspired learning architecture that integrates visual data with somatosensory data from stretchable sensors," *Nature Electronics*, vol. 3, no. 9, pp. 563–570, 2020.

[6] K. S. Abhishek, L. C. F. Qubeley, and D. Ho, "Glove-based hand gesture recognition sign language translator using capacitive touch sensor," in *2016 IEEE international conference on electron devices and solid-state circuits (EDSSC)*. IEEE, 2016, pp. 334–337.

[7] L. Tang, J. Shang, and X. Jiang, "Multilayered electronic transfer tattoo that can enable the crease amplification effect," *Science Advances*, vol. 7, no. 3, p. eabe3778, 2021.

[8] K. K. Kim, M. Kim, K. Pyun, J. Kim, J. Min, S. Koh, S. E. Root, J. Kim, B.-N. T. Nguyen, Y. Nishio *et al.*, "A substrate-less nanomesh receptor with meta-learning for rapid hand task recognition," *Nature Electronics*, vol. 6, no. 1, pp. 64–75, 2023.

[9] P. K. Pisharady and M. Saerbeck, "Recent methods and databases in vision-based hand gesture recognition: A review," *Computer Vision and Image Understanding*, vol. 141, pp. 152–165, 2015.

[10] M. Simao, N. Mendes, O. Gibaru, and P. Neto, "A review on electromyography decoding and pattern recognition for human-machine interaction," *Ieee Access*, vol. 7, pp. 39 564–39 582, 2019.

[11] C. Amma, T. Krings, J. Böer, and T. Schultz, "Advancing muscle-computer interfaces with high-density electromyography," in *Proceedings of the 33rd Annual ACM Conference on Human Factors in Computing Systems*, 2015, pp. 929–938.

[12] Y. Zhang and C. Harrison, "Tomo: Wearable, low-cost electrical impedance tomography for hand gesture recognition," in *Proceedings of the 28th Annual ACM Symposium on User Interface Software & Technology*, 2015, pp. 167–173.

[13] G. Ma, Z. Hao, X. Wu, and X. Wang, "An optimal electrical impedance tomography drive pattern for human-computer interaction applications," *IEEE transactions on biomedical circuits and systems*, vol. 14, no. 3, pp. 402–411, 2020.

[14] Y. Wu, D. Jiang, J. Duan, X. Liu, R. Bayford, and A. Demosthenous, "Towards a high accuracy wearable hand gesture recognition system using eit," in *2018 IEEE International Symposium on Circuits and Systems (ISCAS)*. IEEE, 2018, pp. 1–4.

[15] J. Yao, H. Chen, Z. Xu, J. Huang, J. Li, J. Jia, and H. Wu, "Development of a wearable electrical impedance tomographic sensor for gesture recognition with machine learning," *IEEE journal of biomedical and health informatics*, vol. 24, no. 6, pp. 1550–1556, 2019.

[16] B. B. Atitallah, Z. Hu, D. Bouchaala, M. A. Hussain, A. Ismail, N. Derbel, and O. Kanoun, "Hand sign recognition system based on eit imaging and robust cnn classification," *IEEE Sensors Journal*, vol. 22, no. 2, pp. 1729–1737, 2021.

[17] X. Lu, S. Sun, K. Liu, J. Sun, and L. Xu, "Development of a wearable gesture recognition system based on two-terminal electrical impedance tomography," *IEEE Journal of Biomedical and Health Informatics*, vol. 26, no. 6, pp. 2515–2523, 2021.

[18] J. Avery, T. Dowrick, M. Faulkner, N. Goren, and D. Holder, "A versatile and reproducible multi-frequency electrical impedance tomography system," *Sensors*, vol. 17, no. 2, p. 280, 2017.

[19] F. Santosa and M. Vogelius, "A backprojection algorithm for electrical impedance imaging," *SIAM Journal on Applied Mathematics*, vol. 50, no. 1, pp. 216–243, 1990.

[20] E. Zheng, Y. Li, Z. Zhao, Q. Wang, and H. Qiao, "An electrical impedance tomography based interface for human–robot collaboration," *IEEE/ASME Transactions on Mechatronics*, vol. 26, no. 5, pp. 2373–2384, 2020.

[21] S. Inc., "Shieldex technik-tex p180 + b," 2024. [Online]. Available: https://www.shieldex.de/en/products/shieldex-technik-tex-p180-b/

[22] R. J. Dave, X. Min, Z. Lou, and R. Stewart, "Investigating construction and integration techniques of dry silver-based textile electrodes on electromyography of biceps brachii muscle," *Engineering Proceedings*, vol. 52, no. 1, p. 21, 2024.

[23] M. Min, M. Lehti-Polojärvi, J. Hyttinen, M. Rist, R. Land, and P. Annus, "Bioimpedance spectro-tomography system using binary multifrequency excitation," *International Journal of Bioelectromagnetism*, vol. 209, pp. 76–79, 2018.

[24] A. Dementyev and J. A. Paradiso, "Wristflex: low-power gesture input with wrist-worn pressure sensors," in *Proceedings of the 27th annual ACM symposium on User interface software and technology*, 2014, pp. 161–166.

[25] V. Kolehmainen, M. Lassas, and P. Ola, "Electrical impedance tomography problem with inaccurately known boundary and contact impedances," *IEEE transactions on medical imaging*, vol. 27, no. 10, pp. 1404–1414, 2008.

[26] B. Wang, G. Matcuk, and J. Barbic, "Hand mri dataset," http://www.jernejbarbic.com/hand-mri-dataset.

[27] T. F. O'Connor, M. E. Fach, R. Miller, S. E. Root, P. P. Mercier, and D. J. Lipomi, "The language of glove: Wireless gesture decoder with low-power and stretchable hybrid electronics," *PloS one*, vol. 12, no. 7, p. e0179766, 2017.

[28] D. Kim, O. Hilliges, S. Izadi, A. D. Butler, J. Chen, I. Oikonomidis, and P. Olivier, "Digits: freehand 3d interactions anywhere using a wrist-worn gloveless sensor," in *Proceedings of the 25th annual ACM symposium on User interface software and technology*, 2012, pp. 167–176.

[29] D. Way and J. Paradiso, "A usability user study concerning free-hand microgesture and wrist-worn sensors," in *2014 11th International Conference on Wearable and Implantable Body Sensor Networks*. IEEE, 2014, pp. 138–142.

[30] M. Faulkner, S. Hannan, K. Aristovich, J. Avery, and D. Holder, "Characterising the frequency response of impedance changes during evoked physiological activity in the rat brain," *Physiological measurement*, vol. 39, no. 3, p. 034007, 2018.

[31] S. Gabriel, R. Lau, and C. Gabriel, "The dielectric properties of biological tissues: Ii. measurements in the frequency range 10 hz to 20 ghz," *Physics in medicine & biology*, vol. 41, no. 11, p. 2251, 1996.

[32] A. Adler, P. O. Gaggero, and Y. Maimaitijiang, "Adjacent stimulation and measurement patterns considered harmful," *Physiological measurement*, vol. 32, no. 7, p. 731, 2011.

[33] S. Russo, S. Nefti-Meziani, N. Carbonaro, and A. Tognetti, "A quantitative evaluation of drive pattern selection for optimizing eit-based stretchable sensors," *Sensors*, vol. 17, no. 9, p. 1999, 2017.

[34] W. A. Zgallai, *Biomedical signal processing and artificial intelligence in healthcare*. Academic Press, 2020.

[35] M. Abadi, A. Agarwal, P. Barham, E. Brevdo, Z. Chen, C. Citro, G. S. Corrado, A. Davis *et al.*, "TensorFlow: Large-scale machine learning on heterogeneous systems," 2015, software available from tensorflow.org. [Online]. Available: https://www.tensorflow.org/

[36] X. Glorot and Y. Bengio, "Understanding the difficulty of training deep feedforward neural networks," in *Proceedings of the thirteenth international conference on artificial intelligence and statistics*. JMLR Workshop and Conference Proceedings, 2010, pp. 249–256.

[37] H. Chen, G. Ma, P. Wang, and X. Wang, "A bio-impedance analysis method based on human hand anatomy for hand gesture recognition," *IEEE Transactions on Instrumentation and Measurement*, vol. 70, pp. 1–10, 2021.

[38] Visible Body Suite , "Visible body suite." [Online]. Available: www.visiblebody.com

[39] A. Devices, "Ad5933," 2023. [Online]. Available: https://www.analog.com/en/products/ad5933.html#product-overview

[40] R. J. Halter, A. Hartov, and K. D. Paulsen, "A broadband high-frequency electrical impedance tomography system for breast imaging," *IEEE Transactions on biomedical engineering*, vol. 55, no. 2, pp. 650–659, 2008.

[41] T. E. Kerner, *Electrical impedance tomography for breast imaging*. Dartmouth College, 2001.

[42] N. Avis and D. Barber, "Image reconstruction using non-adjacent drive configurations (electric impedance tomography)," *Physiological measurement*, vol. 15, no. 2A, p. A153, 1994.

[43] C. Xu, X. Dong, X. Shi, F. Fu, W. Shuai, R. Liu, and F. You, "Comparison of drive patterns for single current source eit in computational phantom," in *2008 2nd International Conference on Bioinformatics and Biomedical Engineering*. IEEE, 2008, pp. 1500–1503.

[44] Y. Hochberg and A. Tamhane, *Multiple Comparison Procedures*. John Wiley, 1987.

[45] P. Wei, Z. Lu, and J. Song, "Variable importance analysis: A comprehensive review," *Reliability Engineering & System Safety*, vol. 142, pp. 399–432, 2015.

[46] D. Li, P. Kang, K. Zhu, J. Li, and P. B. Shull, "Feasibility of wearable ppg for simultaneous hand gesture and force level classification," *IEEE Sensors Journal*, vol. 23, no. 6, pp. 6008–6017, 2023.

[47] B. Fang, C. Wang, F. Sun, Z. Chen, J. Shan, H. Liu, W. Ding, and W. Liang, "Simultaneous semg recognition of gestures and force levels for interaction with prosthetic hand," *IEEE Transactions on Neural Systems and Rehabilitation Engineering*, vol. 30, pp. 2426–2436, 2022.

[48] H.-C. Shin, H. R. Roth, M. Gao, L. Lu, Z. Xu, I. Nogues, J. Yao, D. Mollura, and R. M. Summers, "Deep convolutional neural networks for computer-aided detection: Cnn architectures, dataset characteristics and transfer learning," *IEEE transactions on medical imaging*, vol. 35, no. 5, pp. 1285–1298, 2016.

[49] A. Berthelier, T. Chateau, S. Duffner, C. Garcia, and C. Blanc, "Deep model compression and architecture optimization for embedded systems: A survey," *Journal of Signal Processing Systems*, vol. 93, pp. 863–878, 2021.

[50] A. Bangor, P. T. Kortum, and J. T. Miller, "An empirical evaluation of the system usability scale," *Intl. Journal of Human–Computer Interaction*, vol. 24, no. 6, pp. 574–594, 2008.